Applied Physics A (2023) 129:395
https://doi.org/10.1007/s00339-023-06645-7

Applied Physics A
Materials Science & Processing

A physics-based current–voltage model for organic solar cells using a combined analytical and regression approach

M. L. Inche Ibrahim[1]

Received: 11 January 2023 / Accepted: 11 April 2023 / Published online: 5 May 2023

Abstract
A model that can accurately describe the current–voltage (*J*–*V*) characteristics of organic solar cells (OSCs) is crucial for understanding the operation and improving the performance of OSCs. *J*–*V* models based on analytical methods lack the accuracy due to their inability to consider realistic charge carrier generation and recombination. In this paper, we propose a model for describing and predicting the *J*–*V* characteristics of OSCs using a combination of analytical and regression methods. The proposed model allows us to consider the effects of realistic carrier recombination and generation in obtaining the *J*–*V* characteristics. We verify that the proposed model works very well and demonstrate its usefulness by analyzing the effect of trap-assisted recombination on the *J*–*V* characteristics of OSCs, which cannot be analyzed using existing analytical-based *J*–*V* models. We also show that the proposed *J*–*V* model is considerably more reliable than *J*–*V* models based on established numerical methods such as finite difference methods. Since the proposed *J*–*V* model is significantly more accurate than analytical-based *J*–*V* models and considerably more reliable than numerical-based *J*–*V* models, the proposed *J*–*V* model can be a valuable tool for predicting, analyzing, and improving the performance of OSCs.

Keywords Charge carrier generation · Charge carrier recombination · Current–voltage characteristics · Photovoltaic cells · Power conversion efficiency

1 Introduction

Organic solar cells (OSCs) are an attractive photovoltaic technology to support our energy needs owing to their relatively low production cost. OSCs are also lightweight and highly flexible, and therefore have a great potential to be designed and used for specialized applications, for example as power sources for future wearable devices [1] and biomedical devices [2]. Since the efficiency of OSCs is still low compared with established photovoltaic technologies [3], a further improvement in the performance is needed in order to maximize the benefits that OSCs can offer. A model that can accurately and reliably describe and predict the current–voltage (*J*–*V*) characteristics of OSCs is important, for example, to give accurate insights on the operation of OSCs so that the areas of improvement that should be targeted are correctly identified, and to give accurate predictions on how much performance improvement can be achieved. In order to create a *J*–*V* model that is as accurate as possible, every physical process concerning the charge carriers should be described in the most accurate way possible in the model.

A *J*–*V* model obtained using numerical methods (either finite difference, finite element, or finite volume methods) is regarded as the most accurate since every concerned physical process can be treated in its most realistic form in the model. Numerical-based *J*–*V* models were used by many previous studies to analyze OSCs [4–9]. However, Ref. [10] showed that numerical-based *J*–*V* models may not be reliable. Here, the reliability of a model refers to how consistent and accurate the outputs of a model are in comparison with the outputs that the model is expected to produce based on the assigned inputs. Basically, what Ref. [10] showed is that the outputs produced by a numerical-based *J*–*V* model may not always be the results from the intended input parameters, but can be from adjusted input parameters. As suggested in Ref. [10], this reliability issue could be due to the fact that numerical-based *J*–*V* models for OSCs (or for any solar cells actually) employ numerical schemes that

✉ M. L. Inche Ibrahim
lukmanibrahim@iium.edu.my; mlukmanibrahim@gmail.com

[1] Department of Science in Engineering, Faculty of Engineering, International Islamic University Malaysia, Kuala Lumpur, Malaysia

approximately solve the governing equations by making approximations and simplifications while solving the governing equations. What could happen is that while solving the governing equations, the numerical schemes actively make adjustments in order to attain numerical convergences, and these adjustments could effectively change the input parameters as if different input parameters are assigned.

On the other hand, a *J*–*V* model obtained using analytical methods is very reliable because any approximations and simplifications are made before, not while solving the governing equations. However, an analytical-based *J*–*V* model is less accurate than a numerical-based *J*–*V* model due to the fact that some of the concerned physical processes cannot be treated in their most realistic forms because simplifications must be made to the processes before the governing equations can be solved analytically. In short, we can say that an analytical-based *J*–*V* model is significantly more reliable but significantly less accurate than a numerical-based *J*–*V* model.

One of the fundamental processes that is simplified in existing analytical-based *J*–*V* models is concerning the generation of charge carriers. Previous analytical *J*–*V* models either employed uniform carrier generation profiles [11–14] or simple exponential carrier generation profiles based on the Beer–Lambert law [15–17]. However, the carrier generation profiles in OSCs are not only non-uniform (i.e., vary spatially within the active layer) but also significantly more complex than simple exponential profiles [5, 8]. Furthermore, it has been shown that the carrier generation profile can significantly affect the OSC performance [18–20] and the accuracy in modeling the OSC performance [21]. Due to the importance of using realistic carrier generation profiles, Islam et al. [22] developed a semi-analytical *J*–*V* model, employing a combination of analytical and finite difference methods to include the effect of realistic carrier generation profiles.

Another fundamental process that is neglected or sometimes simplified in existing analytical-based *J*–*V* models is concerning the recombination of charge carriers. For example, several existing analytical-based *J*–*V* models neglect the trap-assisted recombination [11–13, 15, 16], whereas a few existing analytical-based *J*–*V* models employ a simplified expression (i.e., monomolecular recombination) as a substitute for the trap-assisted recombination [14, 17], which is very inaccurate as will be shown later in this paper. The trap-assisted recombination or the Shockley–Read–Hall (SRH) recombination is one of the possible loss mechanisms in OSCs [23, 24] and can significantly affect the performance of OSCs [25–28], and therefore should be treated properly in a *J*–*V* model.

In this paper, we propose a new model for describing the *J*–*V* characteristics of OSCs by employing a combination of analytical and regression methods. Using this combined approach, we are able to create a *J*–*V* model for OSCs that can properly incorporate realistic carrier generation profiles and all possible carrier recombination mechanisms (including the trap-assisted recombination), which cannot be achieved by existing analytical-based *J*–*V* models. Furthermore, since the proposed model does not involve the use of finite numerical schemes, it is significantly more reliable than numerical-based *J*–*V* models. In fact, the proposed model is as reliable as a purely analytical-based *J*–*V* model as will be shown later in this paper. In short, the *J*–*V* model proposed in this paper can be a valuable tool for understanding the operation and improving the performance of OSCs due to its significantly better accuracy compared with analytical-based *J*–*V* models, and due to its significantly better reliability compared with numerical-based *J*–*V* models.

2 The proposed model

This Sect. 2 is divided into four subsections. In Sect. 2.1, we describe the OSC structure considered in this paper and the basic equations that describe the generation, recombination, and transport of free charge carriers. In Sect. 2.2, we describe how the carrier recombination rates are calculated based on the method proposed in Ref. [17] but without describing the details on how to solve the carrier continuity equations (which is described later in Sect. 2.4). In Sect. 2.3, we describe how the current densities are calculated based on the method proposed in Ref. [17] but without describing the details on how to solve the carrier continuity equations (which is described later in Sect. 2.4). In Sect. 2.4, we propose a new model for describing the *J*–*V* characteristics of OSCs by proposing a new method for solving the carrier continuity equations, where the obtained solutions can then be used to obtain the carrier recombination rates and the current densities (and hence the *J*–*V* characteristics).

2.1 Device structure and basic equations

Figure 1 illustrates the OSC structure considered in this paper, which is a basic structure for a bulk heterojunction OSC as similarly considered in previous modeling works such as in Refs. [4, 9, 12, 17]. The active layer is made from a blend of an electron accepting material (called acceptor) and an electron donating material (called donor), and is sandwiched between two electrodes. Light absorption creates excitons in the active layer. When the photogenerated excitons reach the donor–acceptor interface, charge-transfer (CT) states are generally produced. A CT state is basically an electron in the acceptor that still binds with a hole in the donor due to their proximity. A CT state may decay to the ground state (a geminate recombination) or dissociate into a free electron and a free hole [23]. A free electron (hole) can travel inside

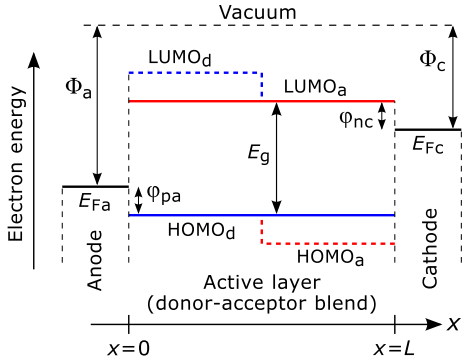

Fig. 1 Schematic illustrating the device structure and the energy levels. $LUMO_d$ and $HOMO_d$ denote the lowest unoccupied molecular orbital (LUMO) and the highest occupied molecular orbital (HOMO) of the donor material, respectively. $LUMO_a$ and $HOMO_a$ denote the LUMO and HOMO of the acceptor material, respectively. E_{Fa} and E_{Fc} denote the Fermi levels of the anode and cathode, respectively. Φ_a and Φ_c denote the work functions of the anode and cathode, respectively. The position $x = 0$ is at the contact between the active layer and the anode while the position $x = L$ is at the contact between the active layer and the cathode

the acceptor (donor) network in order to be collected by the cathode (anode) and generate the desired electrical current. A free electron and a free hole can undergo what is called nongeminate recombination when they encounter each other near the donor–acceptor interface [23, 24]. There are three possible types of nongeminate recombination: nongeminate bimolecular (or Langevin) recombination where a free electron and a free hole recombine to reproduce a CT state [23, 24], trap-assisted recombination or SRH recombination [23, 24], and Auger recombination [24].

The electron and the hole continuity equations inside the active layer ($0 \le x \le L$) at steady state are given by [17]

$$\frac{1}{q}\frac{\partial J_n}{\partial x} + G_n - R_n = 0, \tag{1}$$

$$-\frac{1}{q}\frac{\partial J_p}{\partial x} + G_p - R_p = 0, \tag{2}$$

where q is the elementary charge, J_n (J_p) is the electron (hole) current density, G_n (G_p) is the free electron (hole) generation rate per unit volume due to external photon absorption, and R_n (R_p) is the net nongeminate recombination rate per unit volume for electrons (holes). J_n and J_p are given by

$$J_n = q\mu_n F n + qD_n\frac{\partial n}{\partial x}, \tag{3}$$

$$J_p = q\mu_p F p - qD_p\frac{\partial p}{\partial x}, \tag{4}$$

where μ_n (μ_p) is the electron (hole) mobility, F is the electric field inside the active layer, n (p) is the free electron (hole) concentration, and D_n (D_p) is the electron (hole) diffusion coefficient. In this model, μ_n and μ_p are taken to be uniform (i.e., independent of x). D_n and D_p are given by

$$D_n = \frac{\mu_n k_B T}{q}, \tag{5}$$

$$D_p = \frac{\mu_p k_B T}{q}, \tag{6}$$

where k_B is the Boltzmann constant and T is the absolute temperature (T is assumed uniform). The electric field is also taken to be uniform, and hence, there is no need to consider the Poisson's equation. The uniform electric field is given by [17]

$$F = \frac{V_a - V_{bi}}{L}, \tag{7}$$

where V_a is the applied voltage bias, and L is the active layer thickness. The built-in voltage V_{bi} is given by

$$V_{bi} = \frac{E_g - \varphi_{pa} - \varphi_{nc}}{q}. \tag{8}$$

where E_g (the effective band gap), φ_{pa} (the hole injection barrier at anode), and φ_{nc} (the electron injection barrier at cathode) are as described in Fig. 1.

The nongeminate carrier recombination in OSCs can be due to the Langevin (bimolecular), trap-assisted, and Auger mechanisms [23, 24]. Therefore,

$$R_n = R_p = R_b + R_{trap} + R_A, \tag{9}$$

where R_b is the net nongeminate bimolecular recombination rate per unit volume, R_{trap} is the net trap-assisted recombination rate per unit volume, and R_A is the net Auger recombination rate per unit volume.

The carrier generation originates from the dissociation of CT states, and as described earlier, CT states can be produced from photon absorption (i.e., from photogenerated excitons) and from nongeminate bimolecular recombination. Therefore, G_n and G_p are given by [4, 17]

$$G_n = G_p = P_d\left(G_{CT} + R_b\right), \tag{10}$$

where P_d is the CT state dissociation probability, and G_{CT} is the CT state photogeneration rate per unit volume. Due to the bulk heterojunction design of the active layer, the photogenerated excitons can be assumed to immediately reach the donor–acceptor interface and immediately produce CT states. Hence, the profile of G_{CT} can be assumed to be the same as the light absorption profile. G_{CT} can be obtained

either empirically, through optical modeling, or by assuming a hypothetical profile, depending on the aim of the calculation. The details on how to obtain G_{CT} is out of the scope of this paper.

The CT state dissociation probability is given by

$$P_d = \frac{k_d}{k_d + k_f}, \tag{11}$$

where k_d is the CT state dissociation rate coefficient, and k_f is the CT state decay rate coefficient. Here, we use k_d as proposed in Ref. [29] (which is an improved version of the Onsager–Braun model [30]), which is given by

$$k_d = \frac{3q\left(\mu_{na} + \mu_{pa}\right)}{4\pi\varepsilon a^3} \exp\left(\frac{-E_b}{k_B T}\right) \frac{J_1\left(2\sqrt{-2b_{eff}}\right)}{\sqrt{-2b_{eff}}}, \tag{12}$$

where μ_{na} is the actual electron mobility, μ_{pa} is the actual hole mobility, ε is the effective permittivity of the active layer, a is the electron–hole separation of the CT state, $E_b = q^2/(4\pi\varepsilon a)$ is the binding energy of the CT state, J_1 is the Bessel function of the first kind of order 1, and b_{eff} is given by

$$b_{eff} = \frac{q^3 \lambda |F|}{8\pi\varepsilon\left(k_B T\right)^2}, \tag{13}$$

where $|F|$ is the magnitude of the electric field, and λ is the donor–acceptor morphology parameter. In this model, all parameters that describe k_d are taken to be uniform, and hence, P_d is uniform since both k_d and k_f are uniform here. It is worth mentioning that other models to describe P_d can also be used instead, and P_d does not have to be uniform for this proposed J–V model to work.

The boundary conditions for the carriers at $x = 0$ and $x = L$ are given by [4, 17]

$$n|_{x=0} = N_c \exp\left[\frac{-\left(E_g - \varphi_{pa}\right)}{k_B T}\right], \tag{14}$$

$$n|_{x=L} = N_c \exp\left(\frac{-\varphi_{nc}}{k_B T}\right), \tag{15}$$

$$p|_{x=0} = N_v \exp\left(\frac{-\varphi_{pa}}{k_B T}\right), \tag{16}$$

$$p|_{x=L} = N_v \exp\left[\frac{-\left(E_g - \varphi_{nc}\right)}{k_B T}\right], \tag{17}$$

where N_c (N_v) is the effective density of states in the conduction (valence) band of the acceptor (donor).

2.2 Calculating the carrier recombination rates

To calculate the nongeminate carrier recombination rates, we employ the method proposed in Ref. [17]. In Ref. [17], the free electron (hole) concentration obtained from the solution to the electron (hole) continuity equation that excludes the nongeminate recombination component is called the maximum electron (hole) concentration n_{max} (p_{max}). By excluding the nongeminate recombination, the electron and the hole continuity equations at steady state inside the active layer are given by [17]

$$D_n \frac{\partial^2 n_{max}}{\partial x^2} + \mu_n F \frac{\partial n_{max}}{\partial x} + P_d G_{CT} = 0, \tag{18}$$

$$D_p \frac{\partial^2 p_{max}}{\partial x^2} - \mu_p F \frac{\partial p_{max}}{\partial x} + P_d G_{CT} = 0. \tag{19}$$

Since the derivatives of the unknown functions (i.e., n_{max} and p_{max}) are only with respect to x, Eqs. (18) and (19) are basically nonhomogeneous second-order linear ordinary differential equations (ODEs) with constant coefficients [31]. A nonhomogeneous term for a linear ODE can be defined as a term that does not contain the function to be solved in that ODE [31]. In this case, $P_d G_{CT}$ is the nonhomogeneous term for both Eqs. (18) and (19). The boundary conditions for Eq. (18) are $n_{max}|_{x=0} = n|_{x=0}$ [see Eq. (14)] and $n_{max}|_{x=L} = n|_{x=L}$ [see Eq. (15)], whereas the boundary conditions for Eq. (19) are $p_{max}|_{x=0} = p|_{x=0}$ [see Eq. (16)] and $p_{max}|_{x=L} = p|_{x=L}$ [see Eq. (17)]. We need to find the analytical expressions for n_{max} and p_{max} in order to calculate the nongeminate recombination rates. However, Eqs. (18) and (19) may or may not be able to be solved analytically depending on the function that defines the nonhomogeneous term $P_d G_{CT}$. In this paper, we will propose a method to ensure that the analytical expressions for n_{max} and p_{max} can always be accurately obtained, which will be described later in Sect. 2.4.

According to Ref. [17], n_{max} (p_{max}) is viewed as the number of free electrons (holes) per unit volume that is available to take part in the nongeminate recombination. Therefore, the nongeminate recombination rates are calculated using n_{max} and p_{max} according to Ref. [17]. Using the obtained analytical expressions for n_{max} and p_{max}, we can calculate the net nongeminate bimolecular recombination rate per unit volume, which is given by [4, 17, 32, 33]

$$R_b = \gamma k_L \left(n_{max} p_{max} - n_0 p_0\right), \tag{20}$$

where γ is the bimolecular recombination reduction coefficient, and $k_L = q\left(\mu_n + \mu_p\right)/\varepsilon$ is the Langevin recombination coefficient. The parameter γ has a possible value between 0 and 1 (i.e., $0 \le \gamma \le 1$), and it represents the experimentally observed reduction in the bimolecular recombination coefficient in comparison with the Langevin recombination

coefficient [24, 34]. As for n_0 and p_0, their product is conventionally given by n_{int}^2 where n_{int} is the intrinsic carrier concentration [4, 32, 33]. In this paper, we use n_0p_0 as proposed in Ref. [32]. Note that the use of either n_0p_0 as proposed in Ref. [32] or as conventionally given by $n_0p_0 = n_{\text{int}}^2$ does not affect the validity of the proposed J–V model and the results in this paper.

Similarly, using the obtained analytical expressions for $n_{\max}$ and $p_{\max}$, we can calculate the net trap-assisted recombination rate per unit volume, which is given by [32, 33]

$$R_{\text{trap}} = \frac{v_{\text{th}}\sigma_{\text{n}}\sigma_{\text{p}}N_{\text{trap}}\left(n_{\max}p_{\max} - n_0p_0\right)}{\sigma_{\text{n}}\left(n_{\max} + n_1\right) + \sigma_{\text{p}}\left(p_{\max} + p_1\right)}, \tag{21}$$

where v_{th} is the electron thermal velocity, σ_{n} is the electron capture cross section, σ_{p} is the hole capture cross section, and N_{trap} is the trap density. n_1 and p_1 are given by

$$n_1 = N_{\text{c}} \exp\left(\frac{E_{\text{trap}} - \text{LUMO}_{\text{a}}}{k_{\text{B}}T}\right), \tag{22}$$

$$p_1 = N_{\text{v}} \exp\left(\frac{\text{HOMO}_{\text{d}} - E_{\text{trap}}}{k_{\text{B}}T}\right), \tag{23}$$

where E_{trap} is the trap energy level.

Similarly, using the obtained $n_{\max}$ and $p_{\max}$, we can calculate the net Auger recombination rate per unit volume R_{A}, which is given by [24, 32, 33]

$$R_{\text{A}} = \left(k_{\text{A1}}n_{\max} + k_{\text{A2}}p_{\max}\right)\left(n_{\max}p_{\max} - n_0p_0\right), \tag{24}$$

where k_{A1} and k_{A2} are the Auger recombination coefficients.

2.3 Calculating the current densities

To calculate the current densities, we also employ the method proposed in Ref. [17]. In Ref. [17], the free electron (hole) concentration obtained from the solution to the electron (hole) continuity equation that contains all components, including the nongeminate recombination, is called the net electron (hole) concentration n_{net} (p_{net}). With all components considered, the electron and the hole continuity equations at steady state inside the active layer are given by [17]

$$D_{\text{n}}\frac{\partial^2 n_{\text{net}}}{\partial x^2} + \mu_{\text{n}}F\frac{\partial n_{\text{net}}}{\partial x} + P_{\text{d}}\left(G_{\text{CT}} + R_{\text{b}}\right) - R_{\text{n}} = 0, \tag{25}$$

$$D_{\text{p}}\frac{\partial^2 p_{\text{net}}}{\partial x^2} - \mu_{\text{p}}F\frac{\partial p_{\text{net}}}{\partial x} + P_{\text{d}}\left(G_{\text{CT}} + R_{\text{b}}\right) - R_{\text{p}} = 0. \tag{26}$$

In Eqs. (25) and (26) above, $P_{\text{d}}\left(G_{\text{CT}} + R_{\text{b}}\right)$ are basically G_{n} and G_{p}, respectively [see Eq. (10)], whereas R_{n} and R_{p} are given by the sum of R_{b}, R_{trap}, and R_{A} [see Eq. (9)]. Note that Eqs. (25) and (26) are also nonhomogeneous second-order linear ODEs with constant coefficients. The boundary conditions for Eq. (25) are $n_{\text{net}}\big|_{x=0} = n\big|_{x=0}$ [see Eq. (14)] and $n_{\text{net}}\big|_{x=L} = n\big|_{x=L}$ [see Eq. (15)], whereas the boundary conditions for Eq. (26) are $p_{\text{net}}\big|_{x=0} = p\big|_{x=0}$ [see Eq. (16)] and $p_{\text{net}}\big|_{x=L} = p\big|_{x=L}$ [see Eq. (17)]. We need to find the analytical expressions for n_{net} and p_{net} in order to calculate the current densities. However, Eqs. (25) and (26) may or may not be able to be solved analytically depending on the nonhomogeneous terms. The method to ensure that the analytical expressions for n_{net} and p_{net} can always be accurately obtained will be proposed and described next in Sect. 2.4.

According to Ref. [17], n_{net} (p_{net}) is viewed as the number of free electrons (holes) per unit volume that is available to contribute in generating the electron (hole) current density. Therefore, the electron current density J_{n} and the hole current density J_{p} are calculated using n_{net} and p_{net}, which are given by [17]

$$J_{\text{n}} = q\mu_{\text{n}}Fn_{\text{net}} + qD_{\text{n}}\frac{\partial n_{\text{net}}}{\partial x}, \tag{27}$$

$$J_{\text{p}} = q\mu_{\text{p}}Fp_{\text{net}} - qD_{\text{p}}\frac{\partial p_{\text{net}}}{\partial x}. \tag{28}$$

The total current density J is given by

$$J = J_{\text{n}} + J_{\text{p}}. \tag{29}$$

Note that J must be uniform inside the active layer. The value of J can be obtained by first evaluating J_{n} and J_{p} at any given point inside the active layer, say at $x = L/2$, and then add the obtained values of J_{n} and J_{p}.

2.4 The proposed method

For any nonhomogeneous linear ODEs with constant coefficients [e.g., Eqs. (18), (19), (25), and (26)], the nonhomogeneous terms determine whether the ODEs can be solved analytically or not. This means that in order to analytically solve nonhomogeneous linear ODEs with constant coefficients, the nonhomogeneous terms must be written in the forms that would allow the ODEs to be solved analytically. Here, we propose a simple method for obtaining analytical expressions that can accurately describe the solutions to any nonhomogeneous linear ODEs with constant coefficients even if the ODEs originally cannot be solved analytically. The method is to re-express the relevant nonhomogeneous term(s) of the concerned ODE in a new form that would still accurately describes the original ODE within its domain, but now allows the ODE to be solved analytically.

To explain the proposed method, consider solving Eqs. (25) and (26). Suppose that Eqs. (25) and (26) cannot be

solved analytically due to the nonhomogeneous term R_{trap}. Let us rewrite Eqs. (25) and (26) as

$$D_n \frac{\partial^2 n_{net}}{\partial x^2} + \mu_n F \frac{\partial n_{net}}{\partial x} + P_d G_{CT} - R_c = 0, \tag{30}$$

$$D_p \frac{\partial^2 p_{net}}{\partial x^2} - \mu_p F \frac{\partial p_{net}}{\partial x} + P_d G_{CT} - R_c = 0, \tag{31}$$

where R_c is the combined net carrier recombination rate per unit volume, given by

$$R_c = \left(1 - P_d\right) R_b + R_{trap} + R_A. \tag{32}$$

In order to obtain analytical solutions to the ODEs of Eq. (30) [or Eq. (25)] and Eq. (31) [or Eq. (26)], we need to re-express R_{trap} in a suitable form such that the ODEs can be solved analytically. Here, we propose the use of polynomial regression to re-express R_{trap} in the form of a polynomial of degree m (denoted as P_m) given by

$$P_m(x) = \sum_{k=0}^{k=m} a_k x^k, \tag{33}$$

where the coefficients of the polynomial (i.e., a_k) are obtained through least-squares fitting to the original values of R_{trap} (the original values of R_{trap} are the values of R_{trap} extracted from the original form or expression of R_{trap}). In order to accurately re-express R_{trap} in the form described by Eq. (33), the degree m must be high enough (a higher m leads to a better fitting, but as will be shown later, $m = 7$ is generally adequate), the number of input points or input values used in the fitting must also be high enough, and the input points must be well distributed within the domain of R_{trap} (i.e., within $0 \le x \le L$). The fitting can be easily done using a mathematical software (e.g., using an in-built function called polyfit in MATLAB). Once R_{trap} in the form of P_m is obtained and used in Eqs. (30) and (31), we can then analytically solve those ODEs, which can also be done using MATLAB for example (using the diff function). It is worth noting that we can also combine R_{trap} with other nonhomogeneous terms and re-express the combined nonhomogeneous term in the form described by Eq. (33). For example, we can re-express R_c [refer Eq. (32)] in the form given by Eq. (33) in order to analytically solve Eqs. (30) and (31) although we can still analytically solve those ODEs even if $\left(1 - P_d\right) R_b$ and R_A are kept in their original forms. The method described above can be similarly applied to find accurate analytical expressions for n_{max} and p_{max} in case Eqs. (18) and (19) cannot be solved analytically if the original form of $P_d G_{CT}$ is used in those ODEs.

It is worth mentioning that without the method proposed in this paper, the *J–V* model described in this paper is reduced to our previous analytical *J–V* model [17] where realistic G_{CT} profiles and R_{trap} cannot be considered in our previous model since the continuity equations cannot be solved analytically when realistic G_{CT} profiles and R_{trap} are used. Note that our previous *J–V* model [17] was validated with *J–V* data of OSCs whose recombination is dominated by the nongeminate bimolecular recombination. It is also worth mentioning that truncated half-range Fourier series and truncated Taylor series (i.e., Taylor polynomial) may also be used instead of the polynomial described by Eq. (33), but we find that the use of the polynomial described by Eq. (33) is the most practical and the best.

3 Results and discussion

This Sect. 3 is divided into three parts. In Sect. 3.1, we validate the accuracy of the proposed *J–V* model. In Sect. 3.2, we illustrate an advantage of the proposed *J–V* model in comparison with analytical-based *J–V* models by demonstrating the effect of the trap-assisted recombination. In Sect. 3.3, we illustrate an advantage of the proposed *J–V* model in comparison with numerical-based *J–V* models by comparing the reliability of the proposed *J–V* model with the reliability of a standard numerical-based *J–V* model.

3.1 Model validation

To demonstrate the accuracy of the proposed method, and hence the proposed *J–V* model, we will compare between the *J–V* characteristic obtained using R_c in its original form and the *J–V* characteristic obtained using R_c re-expressed in the polynomial form given by Eq. (33) [refer Eq. (32) for R_c]. For the purpose of this comparison, we neglect the effect of R_{trap} by assuming $N_{trap} = 0\ m^{-3}$. The reason R_{trap} is neglected is because Eq. (30) [or Eqs. (25)] and (31)] [or Eq. (26)] cannot be solved analytically to obtain the total current density J if the original form of R_{trap} is used, and hence the above-mentioned comparison cannot be made since the *J–V* characteristic obtained using the original form of R_c would not be available. We also neglect R_A since the effect of R_A in OSCs is generally negligible [24]. Table 1 shows the parameter values used in all calculations unless specified otherwise. The parameter values in Table 1 are mostly the same as used in Ref. [17], which are typical for OSCs, except for the value of γ which is considerably higher but is still valid (the reason for the relatively high γ used here will be explained later). MATLAB is used to perform polynomial regression and analytically solve the continuity equations.

For G_{CT}, we use

$$G_{CT} = G_0 \left(\frac{x}{L}\right)^3 \left[1 - \left(\frac{x}{L}\right)^2\right]^6, \tag{34}$$

Table 1 Parameter values used in all calculations unless specified otherwise

Parameter description (symbol)	Value
Effective band gap (E_g)	1.1 eV
Effective density of states (N_c, N_v)	2×10^{26} m^{-3}
Electron mobility (μ_n)	1.8×10^{-7} m^{2}V^{-1} s^{-1}
Actual electron mobility (μ_{na})	$200\mu_n$
Hole mobility (μ_p)	2.8×10^{-8} m^{2}V^{-1} s^{-1}
Actual hole mobility (μ_{pa})	$200\mu_p$
Effective permittivity (ε)	3×10^{-11} F·m^{-3}
Injection barriers (φ_{pa}, φ_{nc})	0.1 eV
CT state decay rate coefficient (k_f)	1×10^{8} s^{-1}
Electron–hole separation of the CT state (a)	1.8 nm
Temperature (T)	300 K
Active layer thickness (L)	200 nm
Donor–acceptor morphology parameter (λ)	0.2
Bimolecular recombination reduction coefficient (γ)	0.2
Electron thermal velocity (v_{th})	1×10^{5} m·s^{-1}
Electron capture cross section (σ_n)	2×10^{-18} m^2
Hole capture cross section (σ_p)	2×10^{-18} m^2
Trap concentration (N_{trap})	0 m^{-3}
Trap energy level (E_{trap})	0.4 eV below LUMO$_a$
Auger recombination coefficients (k_{A1}, k_{A2})	0 m^{6}s^{-1}

where $G_0 = 4.5\times10^{29}$ m^{-3} s^{-1} is used. Equation (34) has a resemblance to the Kumaraswamy distribution [35], and it has a bell-like shape similar to a normal or Gaussian distribution within the domain $0 \le x \le L$. Note that Eq. (34) is essentially a polynomial and does not need to be re-expressed in another form in order to analytically solve Eqs. (18), (19), (30), and (31) (i.e., the continuity equations).

Figure 2 compares the J–V characteristic obtained using $\gamma = 0$ (which makes $R_b = 0$ [see Eq. (20)], and hence $R_c = 0$ [see Eq. (32)] since R_{trap} and R_A are neglected) with the J–V characteristic obtained using $\gamma = 0.2$. For the calculations shown in Fig. 2, the original forms of R_b and G_{CT} are used since the continuity equations can be solved analytically using the original forms of the nonhomogeneous terms. Figure 2 basically shows that there is a very significant difference between the J–V characteristics obtained using $\gamma = 0$ and $\gamma = 0.2$. This means that when $\gamma = 0.2$ is used (or when the parameter values as shown in Table 1 are used), the calculated J–V characteristic is strongly influenced by R_b (and hence by R_c too). In other words, the calculated J–V characteristic is very sensitive to any changes in R_c when the parameter values as shown in Table 1 are used, and this fact is important in verifying the accuracy of the proposed model next.

Figure 3 compares between the values of R_c obtained using the original expression of R_c and the values of R_c

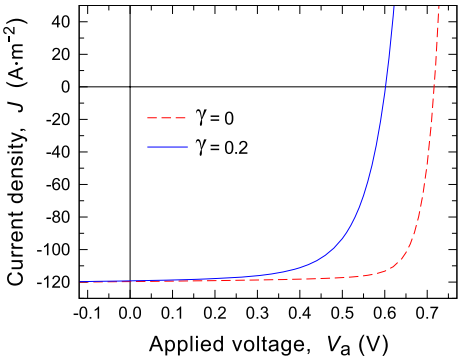

Fig. 2 J–V characteristics for the case $\gamma = 0$ (dashed line) and the case $\gamma = 0.2$ (solid line). The other parameter values used in the calculations are as shown in Table 1

obtained using R_c that is re-expressed in the form of P_m as described by Eq. (33). It can be seen in Fig. 3a that re-expressing R_c in the form of P_7 is adequate to well reproduce the original R_c.

In Fig. 4, it can be seen that using the re-expressed R_c in the form of P_7 gives a J–V characteristic that can very well reproduce the J–V characteristic obtained using the original form of R_c. We find that when R_c in the form of P_7 and R_c in the form of P_{14} are used, the obtained J–V characteristics are

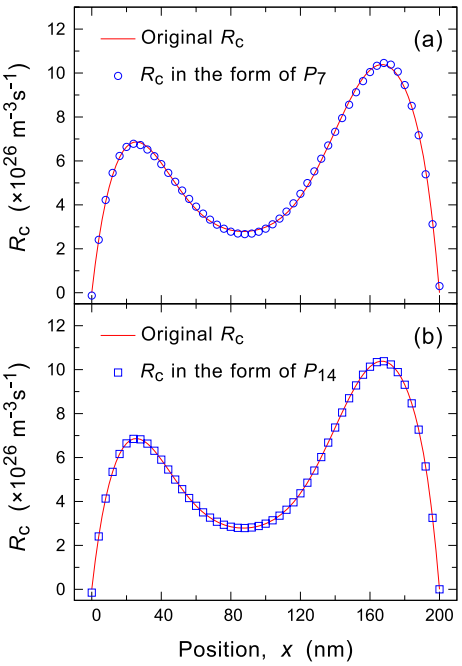

Fig. 3 **a** A comparison between the original R_c, shown by the solid line, and R_c represented in the form of P_7 ($m = 7$) as described by Eq. (33), shown by the circles. **b** A comparison between the original R_c, shown by the solid line, and R_c represented in the form of P_{14} ($m = 14$) as described by Eq. (33), shown by the squares. R_c is given by Eq. (32). All calculations are performed using the parameter values shown in Table 1 at $V_a = 0.47$ V (at the maximum power point)

accurate up to three and nine significant figures, respectively, when compared with the *J*–*V* characteristic obtained using the original R_c. It is important to note that the *J*–*V* characteristics given by the solid lines in Fig. 4 (i.e., obtained using the original form of R_c) are essentially the *J*–*V* characteristics obtained using our previously validated analytical *J*–*V* model [17] (see the explanation at the end of Sect. 2.4). It is worth recalling that the *J*–*V* characteristics in Fig. 4 (using the parameter values in Table 1) should be sensitive to any inaccuracies that may occur in the process of re-expressing R_c from the original form to the form of Eq. (33). Therefore, the results shown in Figs. 3 and 4 conclusively prove that the method, and hence *J*–*V* model proposed here, works very well.

3.2 The effect of trap-assisted recombination

To exemplify the usefulness of the proposed *J*–*V* model, we will use the proposed *J*–*V* model to analyze the effect of the trap-assisted recombination on the *J*–*V* characteristics of OSCs. We use the same parameter values as shown in Table 1 except for N_{trap}, where $N_{trap} = 1 \times 10^{19}$ m^{-3} is used. As shown in Fig. 5, the existence of R_{trap} affects the *J*–*V* characteristic from the short-circuit up to the open-circuit (compare the dashed line with the solid line), and this is unlike the effect of R_b which is negligible around the short-circuit condition [refer Fig. 2 and compare the difference between the use of $\gamma = 0$ (no R_b) and $\gamma = 0.2$ (R_b exists significantly)].

In previous analytical *J*–*V* models [14, 17], the nongeminate monomolecular recombination is used as a simplification and replacement for the trap-assisted recombination. To investigate the accuracy of this simplification, we compare between the *J*–*V* characteristic obtained using the trap-assisted recombination and the *J*–*V* characteristic obtained using the monomolecular recombination. The net nongeminate monomolecular recombination rate per unit volume R_m is given by [17]

$$R_m = k_{mn}\left(n_{max} - n_0\right) = k_{mp}\left(p_{max} - p_0\right), \tag{35}$$

where k_{mn} (k_{mp}) is the monomolecular recombination coefficient for electrons (holes). As used for the other recombination processes in this paper, n_0 and p_0 as proposed in Ref. [32] are used here. We choose $k_{mn} = 8 \times 10^5$ s^{-1} so that when we replace R_{trap} (where $N_{trap} = 1 \times 10^{19}$ m^{-3}) with R_m, we obtain the same short-circuit current density. By comparing the dotted line with the dashed line in Fig. 5, it is clear that the monomolecular recombination cannot correctly reproduce the effect of the trap-assisted recombination on the *J*–*V* characteristics of OSCs. Therefore, employing the trap-assisted recombination instead of the monomolecular recombination is very important to correctly analyze and predict the performance of OSCs.

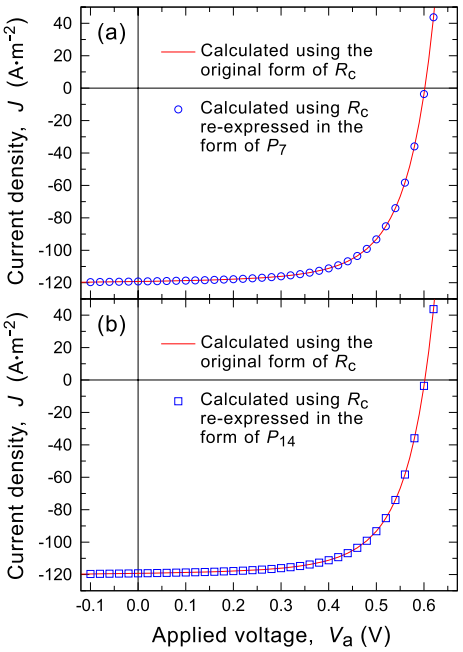

Fig. 4 **a** A comparison between the *J*–*V* characteristics obtained using the original form of R_c, shown by the solid line, and R_c re-expressed in the form of P_7 [see Eq. (33)], shown by the circles. **b** A comparison between the *J*–*V* characteristics obtained using the original form of R_c, shown by the solid line, and R_c re-expressed in the form of P_{14} [see Eq. (33)], shown by the squares. All calculations are performed using the parameter values shown in Table 1

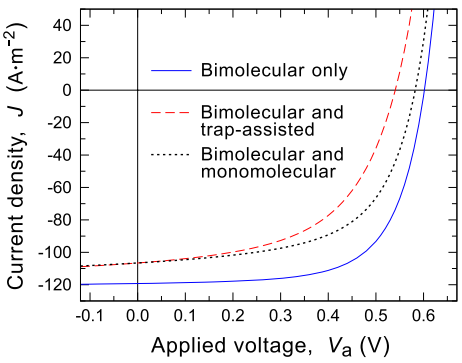

Fig. 5 *J*–*V* characteristics calculated using R_c [see Eq. (32)] re-expressed in the form of P_{14} [see Eq. (33)] when R_c consists of R_b only [thus giving $R_c = (1 - P_d)R_b$] (shown by the solid line), R_c consists of R_b and R_{trap} [thus giving $R_c = (1 - P_d)R_b + R_{trap}$] (shown by the dashed line), and R_c consists of R_b and R_m [thus giving $R_c = (1 - P_d)R_b + R_m$] (shown by the dotted line). R_b, R_{trap}, R_A, and R_m are described by Eqs. (20), (21), (24), and (35), respectively. $N_{trap} = 1 \times 10^{19}$ m^{-3} and $k_{mn} = 8 \times 10^5$ s^{-1} are used in obtaining the dashed line and the dotted line, respectively, while the other parameter values are as shown in Table 1

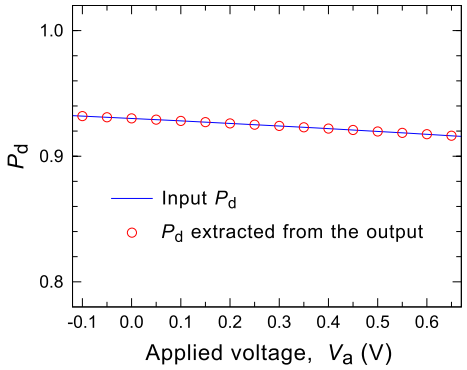

Fig. 6 A comparison between the input P_d [using by Eqs. (11), (12) and (13)], shown by the solid line, and P_d extracted from the output of the proposed *J–V* model [using Eq. (36)], shown by the circles

3.3 Model reliability

To compare the reliability (where the reliability of a model is defined earlier in Sect. 1) of the proposed *J–V* model with the reliability of a standard numerical-based *J–V* model, we will perform an analysis as previously performed in Ref. [10]. To be consistent with the analysis performed in Ref. [10], R_{trap} and R_A are neglected (coincidentally, they are already neglected in Table 1), which gives $R_n = R_b$ [see Eq. (9)]. As mentioned in Sect. 2.1, the CT state dissociation probability P_d is independent of x in this paper, but it does not have to be so for the proposed model to work. By applying Eq. (10) to Eq. (1), and then integratingEq. (1) with respect to x from $x = 0$ to $x = L$, we can then rearrange the resulting integration and get

$$P_d = \frac{J_n|_{x=0} - J_n|_{x=L} + q\int_0^L R_b dx}{q\int_0^L G_{CT} dx + q\int_0^L R_b dx}, \tag{36}$$

where $J_n|_{x=0}$ and $J_n|_{x=L}$ are the output J_n's at $x = 0$ and $x = L$, respectively, G_{CT} is given by Eq. (34), and R_b is given by Eq. (20). If the proposed model is reliable, then the input P_d [see Eqs. (11)–(13)] should be the same as P_d calculated using Eq. (36), which is P_d extracted from the output of the model.

Figure 6 shows that P_d extracted from the output of the proposed *J–V* model is the same as the input P_d that is used to calculate the output. This shows that the output obtained using the proposed *J–V* model is reliable since the model indeed calculates and obtains the output of the intended input. In a previous study, Ref. [10] showed that P_d extracted from the output of a numerical-based *J–V* model and its input P_d are not only significantly different in terms of their values, but also in terms of how they behave as functions of V_a. Therefore, we can conclude that the output produced by the proposed *J–V* model is more reliable (as reliable as an analytical-based *J–V* model) than the output produced by a numerical-based *J–V* model, and as explained earlier in Sect. 1, this is actually not surprising since the proposed *J–V* model makes approximations and simplifications before solving the continuity equations (like a purely analytical-based *J–V* model) whereas a numerical-based *J–V* model makes approximations, simplifications, and adjustments while solving the continuity equations.

4 Conclusion

We have proposed a model for describing the *J–V* characteristics of OSCs using a combination of analytical and regression methods. The proposed *J–V* model allows us to consider all possible nongeminate recombination mechanisms and realistic carrier generation profiles, which cannot be considered by previous analytical-based *J–V* models. We conclusively demonstrated that the proposed *J–V* model works very well. We then used the proposed model to show that the effect of the trap-assisted recombination on the *J–V* characteristics of OSCs cannot be correctly reproduced by replacing it with the monomolecular recombination. This means that it is essential to consider the trap-assisted recombination (which cannot be considered by previous analytical-based *J–V* models), not the monomolecular recombination, when analyzing and predicting the *J–V* characteristics of OSCs whose performance is influenced by the traps. We also showed that the proposed *J–V* model is very reliable and considerably more reliable than a standard numerical-based *J–V* model. Since the proposed *J–V* model is significantly more accurate than analytical-based *J–V* models, and significantly more reliable than numerical-based *J–V* models, the proposed model can be a valuable tool for predicting, analyzing, and improving the performance of OSCs.

Acknowledgements This work was partly supported by the Fundamental Research Grant Scheme (FRGS/1/2017/STG02/UIAM/03/2) from the Ministry of Higher Education of Malaysia.

Data availability The data that support the findings of this study are available within the paper.

References

1. T.F. O'Connor, A.V. Zaretski, S. Savagatrup, A.D. Printz, C.D. Wilkes, M.I. Diaz, E.J. Sawyer, D.J. Lipomi, Sol. Energy Mater. Sol. Cells **144**, 438 (2016)
2. S. Park, S.W. Heo, W. Lee, D. Inoue, Z. Jiang, K. Yu, H. Jinno, D. Hashizume, M. Sekino, T. Yokota, K. Fukuda, K. Tajima, T. Someya, Nature **561**, 516 (2018)
3. "Best Research-Cell Efficiency Chart," NREL.gov. Available: https://www.nrel.gov/pv/cell-efficiency.html. Accessed 24 Dec 2022

4. L.J.A. Koster, E.C.P. Smits, V.D. Mihailetchi, P.W.M. Blom, Phys. Rev. B **72**, 085205 (2005)
5. R. Hausermann, E. Knapp, M. Moos, N.A. Reinke, T. Flatz, B. Ruhstaller, J. Appl. Phys. **106**, 104507 (2009)
6. M.L. Inche Ibrahim, Z. Ahmad, K. Sulaiman, S.V. Muniandy, AIP Adv. **4**, 057133 (2014)
7. J. Kniepert, I. Lange, N.J. van der Kaap, L.J.A. Koster, D. Neher, Adv. Energy Mater. **4**, 1301401 (2014)
8. A.H. Fallahpour, A. Gagliardi, D. Gentilini, A. Zampetti, F. Santoni, M. Auf der Maur, A. Di Carlo, J. Comput. Electron. **13**, 933 (2014)
9. C.H. Kim, J. Choi, Y. Bonnassieux, G. Horowitz, J. Comput. Electron. **15**, 1095 (2016)
10. M.L. Inche Ibrahim, J. Appl. Phys. **119**, 154504 (2016)
11. M.L. Inche Ibrahim, Z. Ahmad, K. Sulaiman, AIP Adv. **5**, 027115 (2015)
12. S. Altazin, R. Clerc, R. Gwoziecki, G. Pananakakis, G. Ghibaudo, C. Serbutoviez, Appl. Phys. Lett. **99**, 143301 (2011)
13. U. Würfel, D. Neher, A. Spies, S. Albrecht, Nat. Commun. **6**, 6951 (2015)
14. M.M. Chowdhury, M.K. Alam, Curr. Appl. Phys. **14**, 340 (2014)
15. S.M. Arnab, M.Z. Kabir, J. Appl. Phys. **115**, 034504 (2014)
16. L. Torto, A. Cester, A. Rizzo, N. Wrachien, S.A. Gevorgyan, M. Corazza, F.C. Krebs, IEEE J. Electron. Devices Soc. **4**, 387–395 (2016)
17. M.L. Inche Ibrahim, Semicond. Sci. Technol. **33**, 125005 (2018)
18. J. Mescher, N. Christ, S. Kettlitz, A. Colsmann, U. Lemmer, Appl. Phys. Lett. **101**, 073301 (2012)
19. W. Tress, A. Merten, M. Furno, M. Hein, K. Leo, M. Riede, Adv. Energy Mater. **3**, 631 (2013)
20. A.H.I. Mohamed, M.L. Inche Ibrahim, IIUM Eng. J. **22**, 135 (2021)
21. H.A. Hassan, M.L. Inche Ibrahim, J. Phys. Conf. Ser. **1489**, 012019 (2020)
22. M. Islam, S. Wahid, M.M. Chowdhury, F. Hakim, M.K. Alam, Org. Electron. **46**, 226 (2017)
23. A.J. Heeger, Adv. Mater. **26**, 10 (2014)
24. C.M. Proctor, M. Kuik, T.Q. Nguyen, Prog. Polym. Sci. **38**, 1941 (2013)
25. S. Yan, L. Lv, Y. Ning, L. Qin, C. Li, X. Liu, Y. Hu, Z. Lou, F. Teng, Y. Hou, Phys. Status Solidi A **212**, 2169 (2015)
26. S. Zeiske, O.J. Sandberg, N. Zarrabi, W. Li, P. Meredith, A. Armin, Nat. Commun. **12**, 3603 (2021)
27. X. Hao, S. Wang, T. Sakurai, S. Masuda, K. Akimoto, A.C.S. Appl, Mater. Interfaces **7**, 18379 (2015)
28. Z. Chen, T. Wang, Z. Wen, P. Lu, W. Qin, H. Yin, X.T. Hao, ACS Energy Lett. **6**, 3203 (2021)
29. M.L. Inche Ibrahim, J. Phys. D: Appl. Phys. **50**, 065103 (2017)
30. C.L. Braun, J. Chem. Phys. **80**, 4157 (1984)
31. D.G. Zill, M.R. Cullen, *Differential Equations with Boundary-Value Problems*, 7th edn. (Brooks/Cole, California, 2009)
32. M.L. Inche Ibrahim, A.A. Zakhidov, Appl. Phys. A **128**, 21 (2022)
33. S.J. Fonash, *Solar Cell Device Physics*, 2nd edn. (Academic Press, Massachusetts, 2010)
34. G. Juška, K. Arlauskas, J. Stuchlik, R. Österbacka, J. Non-Cryst. Solids **352**, 1167 (2006)
35. P. Kumaraswamy, J. Hydrol. **46**, 79 (1980)